# Doc2-mediated superpriming supports synaptic augmentation

Renhao Xue[a,b], David A. Ruhl[a,b,c], Joseph S. Briguglio[a,b], Alexander G. Figueroa[d], Robert A. Pearce[d], and Edwin R. Chapman[a,b,1]

[a]Howard Hughes Medical Institute, University of Wisconsin–Madison, Madison, WI 53705-2275; [b]Department of Neuroscience, University of Wisconsin–Madison, Madison, WI 53705-2275; [c]Neuroscience Training Program, University of Wisconsin, Madison, WI 53705-2275; and [d]Department of Anesthesiology, University of Wisconsin–Madison, Madison, WI 53705-2275

Edited by Erwin Neher, Max-Planck Institute for Biophysical Chemistry, Goettingen, Germany, and approved May 7, 2018 (received for review February 6, 2018)

**Various forms of synaptic plasticity underlie aspects of learning and memory. Synaptic augmentation is a form of short-term plasticity characterized by synaptic enhancement that persists for seconds following specific patterns of stimulation. The mechanisms underlying this form of plasticity are unclear but are thought to involve residual presynaptic $Ca^{2+}$. Here, we report that augmentation was reduced in cultured mouse hippocampal neurons lacking the $Ca^{2+}$ sensor, Doc2; other forms of short-term enhancement were unaffected. Doc2 binds $Ca^{2+}$ and munc13 and translocates to the plasma membrane to drive augmentation. The underlying mechanism was not associated with changes in readily releasable pool size or $Ca^{2+}$ dynamics, but rather resulted from superpriming a subset of synaptic vesicles. Hence, Doc2 forms part of the $Ca^{2+}$-sensing apparatus for synaptic augmentation via a mechanism that is molecularly distinct from other forms of short-term plasticity.**

short-term plasticity | synaptic augmentation | Doc2 | munc13 | superpriming

Neurons communicate with one another using chemical synapses that typically display plasticity; that is, their strength is modulated in an activity-dependent manner (1). Short-term synaptic plasticity (STP) occurs on timescales of milliseconds to minutes and contributes to a wide range of neuronal functions ranging from working memory to motor control (2–4). Short-term enhancement (STE) refers to an increase, and short-term depression refers to a decrease, in the strength of transmission. Subtypes of STE are typically classified, according to their timescales, into the following: paired pulse facilitation (PPF; milliseconds), augmentation (seconds), and posttetanic potentiation (PTP; minutes) (1, 5–7). These forms of plasticity are thought to depend on residual $Ca^{2+}$, which accumulates in presynaptic nerve terminals during bouts of synaptic activity (1, 8). Hence, $Ca^{2+}$-binding proteins play crucial roles in different forms of STP. For example, synaptotagmin 7 has been shown to mediate PPF (9). Although significant progress has been made, it is still unclear how various presynaptic proteins utilize $Ca^{2+}$ signals to execute different forms of synaptic plasticity.

The focus of the current study is synaptic augmentation. Like other forms of STE, this form of plasticity has been actively studied for decades in cultured neurons (10–13), hippocampal slices (14–16), and the neuromuscular junction (17), yet the underlying mechanisms remain elusive. The synaptic vesicle (SV) priming factor munc13 (18) has been shown to play a role in augmentation (11–13), in part by interacting with calmodulin (12). However, disruption of the calmodulin-binding site of munc13 only partially eliminated augmentation (12), suggesting that additional, unidentified mechanisms exist.

The double C2 domain protein (Doc2) is one such possible contributor to augmentation, as it is a $Ca^{2+}$-binding protein that also interacts with munc13 via its munc13 interaction (MID) domain (19). Two of the three known isoforms of Doc2 (α and β) bind $Ca^{2+}$ and interact with phospholipids and target membrane soluble *N*-ethylmaleimide-sensitive factor attachment protein receptors (SNAREs) in a $Ca^{2+}$-dependent manner. These interactions are mediated via tandem C2 domains (C2A and C2B) (20, 21). Doc2α/β have been proposed to function as $Ca^{2+}$ sensors for asynchronous (22) and spontaneous (23) SV release (but see also refs. 24 and 25). Moreover, Doc2 has been implicated in synaptic plasticity: loss of Doc2α leads to altered synaptic depression during train stimulation (22, 26) and disrupts long-term potentiation (26). However, a role for Doc2 in synaptic augmentation has not been explored.

In the present study, we systematically tested the role of Doc2 in three types of STE in cultured mouse hippocampal neurons. We found that synaptic augmentation, but not PPF or PTP, was impaired in Doc2α/β double knockout (DKO) neurons. Moreover, the ability to bind $Ca^{2+}$ and munc13 underlies the function of Doc2 in augmentation. Finally, we determined that augmentation in cultured hippocampal neurons results from superpriming of a subset of SVs and is not due to an effect on the size of the readily releasable pool (RRP) of SVs or presynaptic $Ca^{2+}$ dynamics. These observations reveal a previously unidentified function for Doc2 in presynaptic nerve terminals and provide insights into the molecular mechanisms that underlie synaptic plasticity.

## Significance

**Plastic changes in synaptic connections constitute the basis of learning and memory. Different forms of synaptic plasticity are generally distinguished experimentally by their timescales, but it is unclear whether each form of plasticity corresponds to a distinct biological process with a dedicated molecular mechanism. In the present study, we show that the $Ca^{2+}$-binding protein, Doc2, "superprimes" a subset of already primed synaptic vesicles to make them more likely to release, and this process selectively contributes to augmentation (on the scale of seconds). The underlying molecular mechanism does not mediate other forms of short-term enhancement (that occur on the timescale of milliseconds or minutes). This work establishes a function of Doc2 in maintaining synaptic plasticity within a narrow time window.**

Author contributions: R.X., R.A.P., and E.R.C. designed research; R.X., D.A.R., J.S.B., and A.G.F. performed research; R.X., R.A.P., and E.R.C. analyzed data; and R.X., J.S.B., and E.R.C. wrote the paper.

The authors declare no conflict of interest.

This article is a PNAS Direct Submission.



[1]To whom correspondence should be addressed. Email: chapman@wisc.edu.

This article contains supporting information online at www.pnas.org/lookup/suppl/doi:10.1073/pnas.1802104115/-/DCSupplemental.

Published online May 29, 2018.

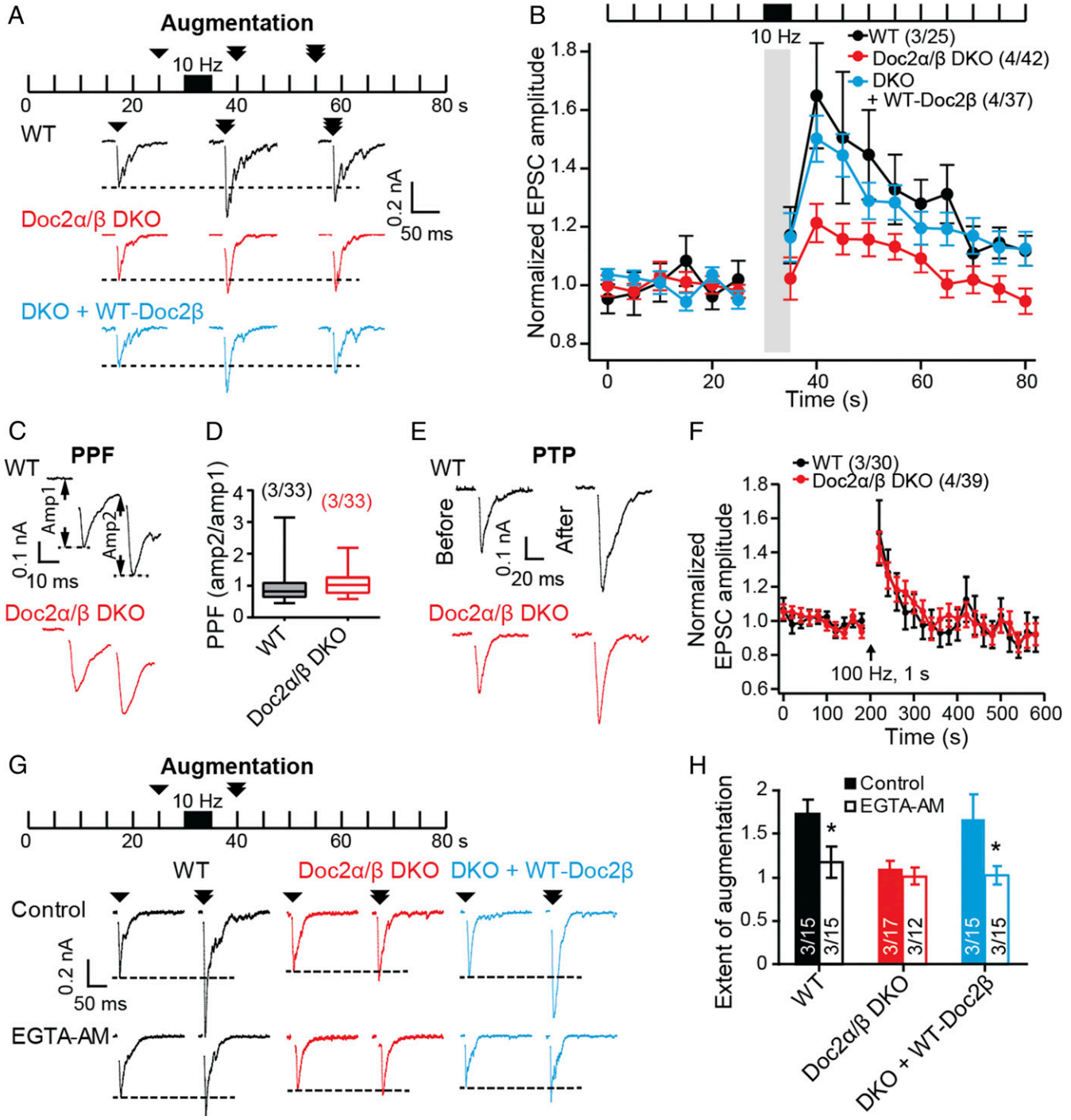


**Fig. 1.** Doc2 selectively regulates synaptic augmentation. (*A*) Test pulses (0.2 Hz) were used to monitor synaptic transmission for 80 s; augmentation was induced via a stimulus train (10 Hz, 5 s) at $t = 30–35$ s. Shown are representative evoked EPSC traces recorded from WT (black), Doc2α/β DKO (red), and DKO neurons expressing WT-Doc2β (light blue), at 25, 40 and 55 s. (*B*) The peak amplitudes of evoked EPSCs were normalized to the baseline and plotted as mean ± SEM; the stimulus train was omitted for clarity (gray bar; detailed in *SI Appendix*, Fig. S1). Augmentation was impaired in Doc2α/β DKO neurons ($P = 0.012$, WT versus DKO, Kruskal–Wallis test followed by Dunn's post hoc test); expression of WT-Doc2β completely rescued augmentation. (*C*) Representative EPSCs showing responses to a paired pulse stimulus (25-ms interval). (*D*) PPF (amplitude of second EPSC over that of the first EPSC) was quantified and graphed using box plots. No difference was found using Mann–Whitney *U* test ($P = 0.0719$). (*E*) Representative EPSC traces recorded before, and 20 s after, PTP was induced via a stimulus train (100 Hz, 1 s). (*F*) The normalized peak amplitudes of evoked EPSCs were quantified and plotted as mean ± SEM. The arrow indicates the stimulus train. WT and Doc2α/β DKO neurons exhibited no differences in PTP. (*G*) WT, Doc2α/β DKO, and DKO neurons expressing WT-Doc2β were pretreated with EGTA-AM (100 μM, 20 min) and subjected to the augmentation protocol as shown in *A*. Shown are representative evoked EPSC traces recorded at 25 and 40 s with (*Lower*) or without (control; *Upper*) EGTA-AM pretreatment. (*H*) Extent of augmentation was calculated as the normalized EPSC amplitude 5 s after the induction train (10 Hz, 5 s). EGTA-AM pretreatment significantly decreased the extent for augmentation in WT neurons and DKO neurons expressing WT-Doc2β, but failed to further reduce augmentation in Doc2α/β DKO neurons. *$P < 0.05$, unpaired *t* test.

## Results

**Synaptic Augmentation Is Reduced in Doc2 Knockout Mice.** To induce augmentation, we stimulated cultured mouse hippocampal neurons at 10 Hz for 5 s (Fig. 1 *A* and *B* and *SI Appendix*, Fig. S1) (10) and subsequently observed a robust increase (65 ± 15%) in the amplitude of excitatory postsynaptic currents (EPSCs) evoked by single-action potentials; this enhancement persisted for tens of seconds in wild-type (WT) cells (Fig. 1*B*). A key finding was that, in Doc2α/β DKO neurons, augmentation was reduced: only a small increase (21 ± 6.7%) in EPSC amplitude was observed ($P < 0.05$, WT versus DKO; Fig. 1*B*). The expression of exogenous Doc2α or -β fully rescued augmentation in Doc2α/β DKO neurons (Fig. 1*B* and *SI Appendix*, Fig. S2 *A* and *B*). These data establish Doc2 as a regulator of synaptic augmentation. This function was specific, as Doc2α/β DKO had little effect on two other forms of STE: PPF and PTP (Fig. 1 *C*–*F*) (26).

To determine whether Doc2 helps drive augmentation via sensing residual $Ca^{2+}$, we pretreated neurons with the membrane-permeable $Ca^{2+}$ chelator EGTA-AM. Consistent with previous studies (11, 12), EGTA-AM pretreatment largely disrupted augmentation in WT neurons (Fig. 1 *G* and *H*). Notably, DKO of Doc2α and -β occluded the effect of EGTA-AM (Fig. 1 *G* and *H*). These findings are consistent with the idea that Doc2 functions as a $Ca^{2+}$ sensor during augmentation.

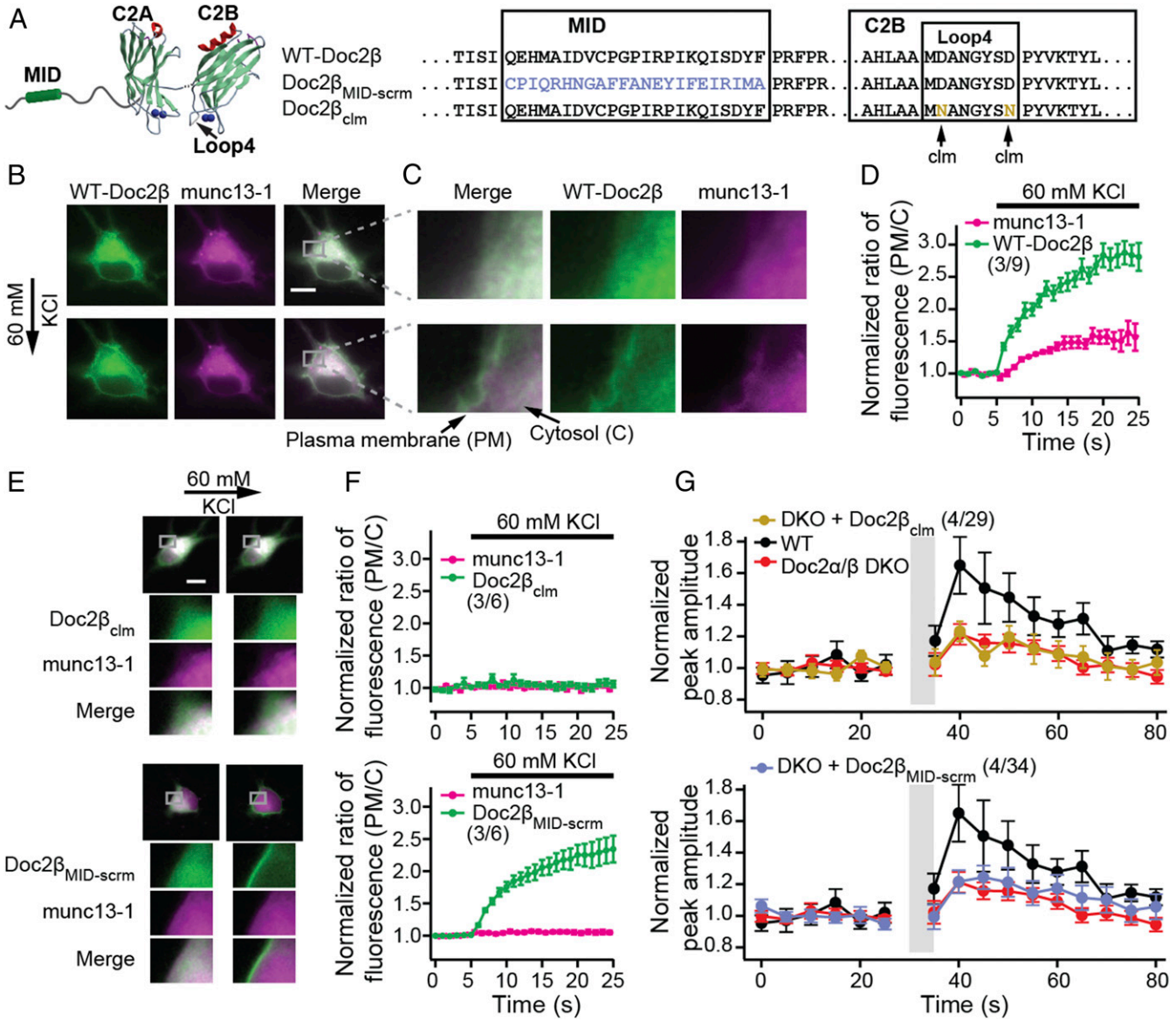


**Fig. 2.** $Ca^{2+}$•Doc2β mediates munc13-1 translocation to the plasma membrane to drive augmentation. (*A*) WT-Doc2β, Doc2β$_{clm}$ in which two acidic $Ca^{2+}$ ligands were neutralized to disrupt $Ca^{2+}$ binding to the C2B domain (clm; $Ca^{2+}$ ligand mutant), and Doc2β$_{MID\text{-}scrm}$ in which the MID domain was scrambled, were expressed in neurons. (*B*) Upon depolarization with 60 mM KCl, both munc13-1–mCherry (magenta) and WT Doc2β-GFP (green) translocated to the plasma membrane. (Scale bar: 10 μm.) (*C*) Magnified images are shown. (*D*) The ratio of fluorescence intensity (plasma membrane/cytosol) was quantified and normalized to baseline, as detailed in *SI Appendix*, Fig. S3, and plotted versus time. (*E*) Upon depolarization, Doc2β$_{clm}$-GFP neither translocates to the plasma membrane nor recruits munc13-1–mCherry (*Upper*); Doc2β$_{MID\text{-}scrm}$-GFP translocates but was also unable to recruit munc13-1–mCherry (*Lower*). (*F*) Translocation data from *E* were quantified and plotted. (*G*) Normalized peak amplitudes of EPSCs before and after the augmentation protocol, as described in Fig. 1, recorded from Doc2α/β DKO neurons expressing Doc2β$_{clm}$ (*Upper*) or Doc2β$_{MID\text{-}scrm}$ (*Lower*) are plotted as mean ± SEM versus time. Data from WT and Doc2α/β DKO neurons (Fig. 1) are shown again as controls. Both Doc2β mutants failed to rescue synaptic augmentation.

**Doc2-Dependent Augmentation Is Mediated by Interactions with $Ca^{2+}$ and Munc13.** In response to increases in intracellular $Ca^{2+}$ concentration ($[Ca^{2+}]_i$), Doc2a/β translocates to the plasma membrane to regulate aspects of exocytosis (27, 28). We therefore addressed the relationship between this $Ca^{2+}$-dependent translocation step and synaptic augmentation. Since both Doc2 isoforms, α or β, can translocate (22, 27) and mediate augmentation (Fig. 1*B* and *SI Appendix*, Fig. S2*B*), we focused on a single isoform, β (Fig. 2*A*). For all translocation experiments, we used both rat hippocampal neurons and PC12 cells; we observed the same effects in both preparations. Depolarization and $Ca^{2+}$ entry triggered robust translocation of Doc2β-GFP to the plasma membrane (Fig. 2 *B–D* and *SI Appendix*, Figs. S3 and S4) (28, 29). Neutralization of two acidic $Ca^{2+}$ ligands in C2B (designated $Doc2\beta_{clm}$; $Ca^{2+}$ ligand mutant; Fig. 2*A*) abolished the ability of this domain to bind $Ca^{2+}$ and disrupted the translocation activity of Doc2 (Fig. 2 *E* and *F* and *SI Appendix*, Fig. S4) (30).

We next addressed the translocation of munc13, which is known to bind Doc2 (19). Interestingly, munc13-1–mCherry also translocated to the plasma membrane in response to $Ca^{2+}$ entry when coexpressed with WT (Fig. 2 *B–D* and *SI Appendix*, Fig. S4; see also ref. 31), but not the $Ca^{2+}$ ligand mutant form, of GFP-tagged Doc2β (Fig. 2 *E* and *F*, *Upper*, and *SI Appendix*, Fig. S4). Hence, the $Ca^{2+}$-dependent translocation of munc13 to the plasma membrane is mediated by Doc2β (the endogenous levels of Doc2 are likely to be too low to drive translocation of the overexpressed munc13 fusion protein). To further address the mechanism of translocation, the MID domain (19) was scrambled (designated as $Doc2\beta_{MID\text{-}scrm}$; Fig. 2*A*) or deleted ($Doc2\beta_{MID\text{-}del}$; *SI Appendix*, Fig. S5) in GFP-Doc2β. Both constructs translocated in response to $Ca^{2+}$ entry but failed to recruit overexpressed munc13-1–mCherry to the plasma membrane (Fig. 2 *E* and *F*, *Lower*, and *SI Appendix*, Figs. S4 and S5 *A* and *B*). Munc13 can also be recruited to the plasma membrane, in a $Ca^{2+}$-independent manner, by phorbol esters (*SI Appendix*, Fig. S6) (32). We observed that phorbol 12-myristate 13-acetate (PMA) resulted in the cotranslocation—with munc13—of WT and the $Ca^{2+}$ ligand mutant form of Doc2β to the plasma membrane, but not the Doc2β mutants that lacked a functional MID domain (*SI Appendix*, Fig. S6; see also refs. 29 and 33). We conclude that these

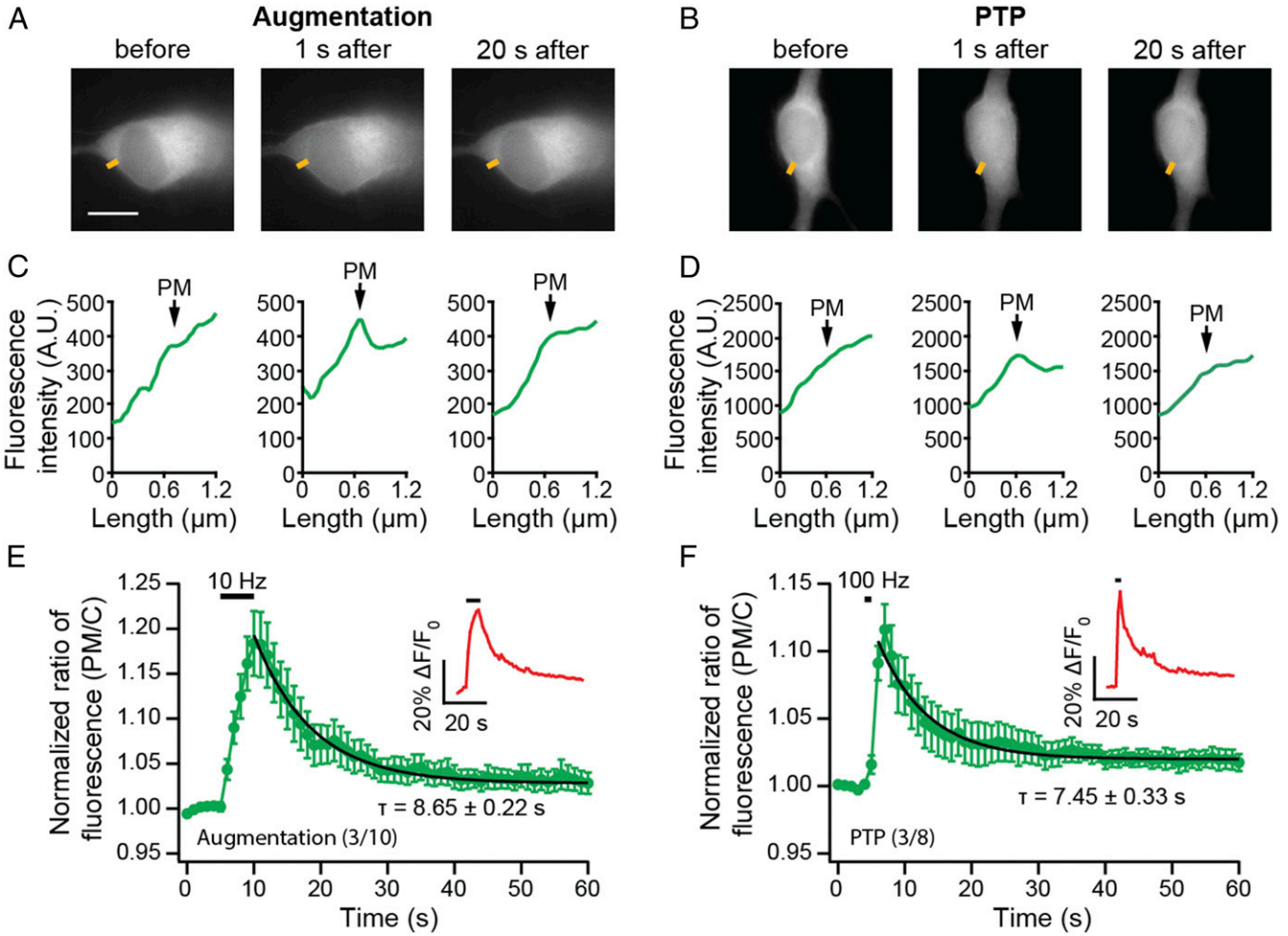


**Fig. 3.** Doc2 dwell time at the plasma membrane coincides with the duration of augmentation. (*A* and *B*) Sample images from neurons stimulated using augmentation (10 Hz, 5 s; *A*) or PTP (100 Hz, 1 s; *B*) protocols. (Scale bar: 10 μm.) Doc2β-GFP translocated to the plasma membrane upon stimulation; after the stimulus train, it retreated back to the cytosol in a time-dependent manner. (*C* and *D*) Under these conditions, low levels of translocation were observed, so representative line scans of Doc2β-GFP fluorescence (yellow line segments in *A* and *B*) are shown; the position of the PM in the line-scan data is indicated. (*E* and *F*) Translocation of Doc2-GFP was quantified using normalized fluorescence intensity ratios (plasma membrane/cytosol), as detailed in *SI Appendix*, Fig. S3. To ensure successful activation of neurons, $[Ca^{2+}]_i$ was monitored during the experiment using X-Rhod-1 AM (averaged trace of normalized fluorescence intensity shown in *Insets*). Single exponential fitting of the averaged traces revealed comparable time constants (τ) for the release of Doc2-GFP from plasma membrane, back to cytosol, following augmentation ($\tau = 8.65 \pm 0.22$ s; *E*) and PTP ($\tau = 7.45 \pm 0.33$ s, *F*).

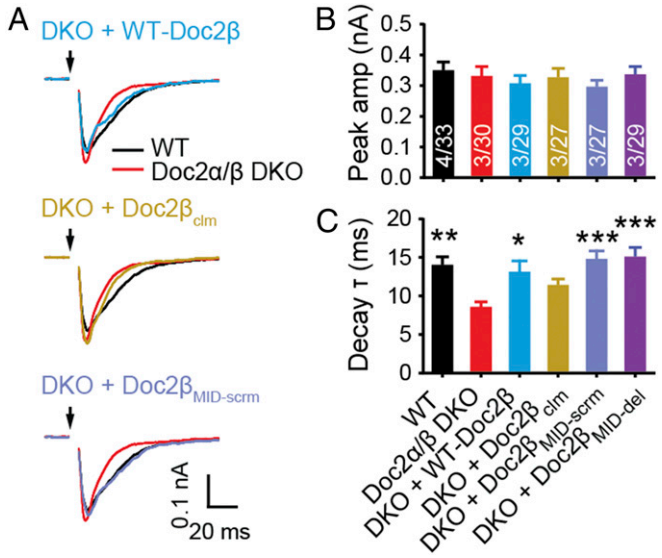


**Fig. 4.** The function of Doc2 in augmentation is independent of its role in asynchronous release. (*A*) Averaged traces of evoked EPSCs; black arrows indicate stimulation. (*B* and *C*) The EPSC amplitude (amp; *B*) and decay time constants (τ; *C*), calculated by fitting the data with single exponential functions, are represented as mean ± SEM. No difference in peak amplitude was found among any group. The decay time constant was fully rescued by expression of $Doc2\beta_{MID\text{-}scrm}$ and $Doc2\beta_{MID\text{-}del}$, but not $Doc2\beta_{clm}$. $^{*}P < 0.05$, $^{**}P < 0.01$, $^{***}P < 0.001$ versus Doc2α/β DKO, Kruskal –Wallis test followed by Dunn's post hoc test.

two proteins interact, to at least some extent, in the cytosol and are recruited to release sites in response to either phorbol esters or increases in $[Ca^{2+}]_i$ (19).

A crucial finding was that $Doc2\beta_{clm}$, which failed to mediate munc13-1 translocation to the plasma membrane in response to $Ca^{2+}$ entry, also failed to rescue augmentation in Doc2α/β DKO neurons (Fig. 2*G*). Similarly, the mutant forms of Doc2 that lacked an intact MID domain also failed to rescue augmentation (Fig. 2*G* and *SI Appendix*, Fig. S5*C*). In all cases, the mutants were expressed at levels comparable to the WT construct (*SI Appendix*, Fig. S7). In summary, these experiments demonstrate that Doc2 binds $Ca^{2+}$ via its C2B domain and munc13 via its MID domain to contribute to synaptic augmentation.

**The Duration of Augmentation Mirrors the Dwell Time of Doc2 at the Plasma Membrane.** The $Ca^{2+}$-driven translocation of Doc2 to the plasma membrane is reversible; after neuronal activation, Doc2β-GFP eventually retreats back to the cytosol (Fig. 3 *A*–*D*). To estimate the dwell time of Doc2β-GFP at the plasma membrane during augmentation, we stimulated neurons electrically, using the same augmentation protocol used in the electrophysiological experiments (Fig. 1). The poststimulation reversal of translocation was monitored via live cell imaging. The relative decrease in signal at the plasma membrane was well-fitted with a single exponential function, yielding a time constant of 8.65 ± 0.22 s (Fig. 3*E*). This value is similar to the duration of synaptic augmentation (10, 14). Interestingly, after a more intense stimulus train that induces PTP (100 Hz, 1 s) (7, 34), Doc2β-GFP retreated from the plasma membrane with similar kinetics (τ = 7.45 ± 0.33 s, Fig. 3*F*) as observed following the augmentation protocol, even though PTP has a much longer duration (minutes). Together, these observations suggest that the dwell time of Doc2 at the plasma membrane determines how long it contributes to synaptic enhancement, temporally defining its role in augmentation.

**Independent Roles of Doc2 in Augmentation and Asynchronous Transmission.** We next determined whether the role of Doc2 in the slow, asynchronous phase of synaptic transmission underlies its function during augmentation. Similar to Doc2α single-KO neurons (22), we found that Doc2α/β DKO neurons exhibited faster evoked EPSC decays (Fig. 4). This was the result of decreased asynchronous SV release and was not due to changes in desensitization of postsynaptic AMPA receptors, as this trend persisted in the presence of cyclothiazide (CTZ), which inhibits desensitization (35, 36) (*SI Appendix*, Fig. S8). We observed that the Doc2 MID domain mutants fully rescued the asynchronous component of neurotransmitter release in Doc2α/β DKO neurons, whereas the $Ca^{2+}$ ligand mutant did not (Fig. 4*C*). Thus, the mechanism by which Doc2 drives asynchronous release is distinct from that of augmentation, since the latter specifically requires the MID domain.

**Doc2-Dependent Augmentation Is Not Mediated via Modulation of RRP Size or Presynaptic $Ca^{2+}$ Dynamics.** In principle, augmentation could result from an increase in the size of the RRP, an increase in release probability ($P_{vr}$), or both. Doc2 has been reported to modulate the size of the RRP in chromaffin cells (37) but not in neurons (22). To validate this observation in neurons, we measured the size of the RRP by applying hypertonic sucrose to trigger release of all primed SVs (38). No differences were found among WT (10), Doc2α/β DKO, and DKO neurons expressing WT and each of the mutant Doc2β constructs, either under resting conditions or following the augmentation protocol (Fig. 5 *A* and *B* and *SI Appendix*, Fig. S9). We confirmed these results using train stimulation to estimate the RRP size (*SI Appendix*, Fig. S10) (39–41). Therefore, Doc2-promoted augmentation is not due to a change in RRP size and is likely due to an increase in $P_{vr}$ (Fig. 5*C*). $P_{vr}$ can be influenced

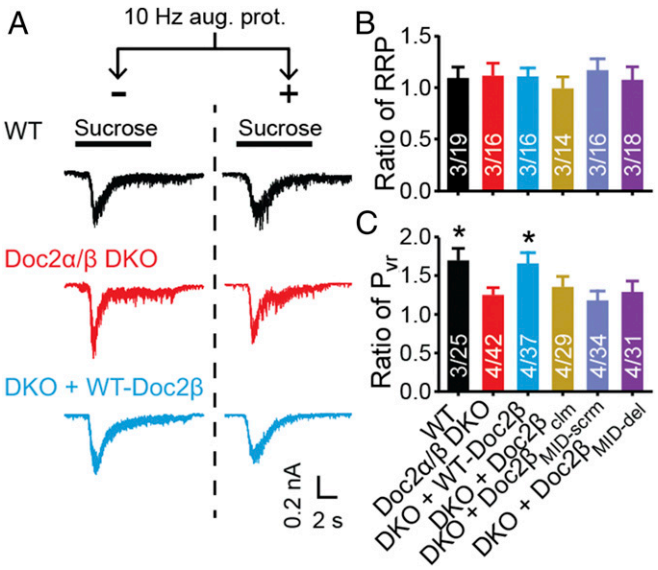


**Fig. 5.** The function of Doc2 in augmentation does not involve changes in the size of the RRP. (*A*) Representative EPSCs, in response to local perfusion with 500 mM sucrose (black bars). (*B*) RRP size was evaluated by integrating the EPSC charge transfer in response to hypertonic sucrose. The RRP ratio was calculated by dividing RRP values obtained with and without augmentation. No significant differences were detected among each group (Kruskal–Wallis test). (*C*) $P_{vr}$ was calculated by normalizing the total charge of evoked EPSCs (Fig. 1) to the RRP. The $P_{vr}$ ratio ($P_{vr}$ after augmentation/$P_{vr}$ before augmentation) was plotted as mean ± SEM, $^{*}P < 0.05$ versus Doc2α/β DKO, Kruskal–Wallis test followed by Dunn's post hoc test. The original data are provided in *SI Appendix*, Fig. S9.

by changes in $Ca^{2+}$ entry or in the likelihood that SVs fuse in response to a given $Ca^{2+}$ concentration. Indeed, a recent study revealed that munc13 can directly regulate $Ca^{2+}$ influx via interactions with voltage-gated $Ca^{2+}$ channels (42). So, we measured $Ca^{2+}$ entry into individual synaptic boutons in WT and Doc2α/β DKO neurons using Fluo-5F before and after the induction of augmentation (Fig. 6*A*) (43). A decrease in the peak $Ca^{2+}$ signal was observed in both genotypes following augmentation, but no significant difference was found between WT and KO neurons after the augmentation protocol (Fig. 6 *B* and *C*). Therefore, the increase in $P_{vr}$ is not due to greater $Ca^{2+}$ entry. It is likely that a pool of munc13, constitutively present at release sites, serves to regulate $Ca^{2+}$ channels while a separate and dynamic pool, regulated by Doc2, has a distinct function during augmentation (44, 45). We note that Doc2α/β DKO neurons exhibited a subtle but significant reduction (~8%) in peak $\Delta F/F_0$ compared with WT before augmentation, whereas no difference was found in the augmented state (Fig. 6 *B* and *C*). The slight reduction in the global $Ca^{2+}$ signal in the KO before augmentation was not associated with changes in EPSC amplitude (Fig. 4*B*), suggesting that $Ca^{2+}$ dynamics might not be affected at release sites, but further work is needed to address this issue.

**Doc2 Promotes Augmentation by Enhancing SV Superpriming.** $P_{vr}$ can be also be elevated by increasing the fraction of "superprimed" SVs (within the RRP), which are more competent for release than normally primed vesicles (34, 46). Superpriming has been reported to underlie PTP (34), but whether it is involved in augmentation remains unknown. In the final series of experiments, we tested the potential role of superpriming in Doc2-regulated augmentation by delivering high-frequency stimulus trains (40 Hz, 0.5 s) to neurons before and after augmentation was induced. As shown in Fig. 7 *A*–*C*, regardless of whether Doc2 was expressed, synapses switch from facilitation to depression following augmentation, indicating an increase in $P_{vr}$. Superprimed SVs are preferentially released during the first few stimuli, but do not impact steady-state EPSC amplitudes during train stimulation (at a sufficiently high frequency) (34). In WT neurons after augmentation, the amplitude of the first three EPSCs increased without any changes in the steady-state EPSCs (Fig. 7 *B*, *C*, *F*, and *G*). We therefore conclude that a larger fraction of SVs become superprimed during the augmentation protocol when Doc2 is expressed. Moreover, as shown in Fig. 7 *C*–*H*, the superpriming phenotype was rescued by WT-Doc2β, but not by mutant forms of Doc2β that failed to rescue augmentation ($Doc2\beta_{clm}$, $Doc2\beta_{MID\text{-}scrm}$, and $Doc2\beta_{MID\text{-}del}$).

## Discussion

Doc2 has been reported to regulate two modes of neurotransmitter release: the slow asynchronous phase of evoked transmission (22, 28) and the spontaneous release of individual synaptic vesicles (23). The present study extends our understanding of this important protein by revealing its mechanism of action during STP. We draw three major conclusions. First, different forms of plasticity, distinguished by different timescales, are likely mediated via distinct molecular mechanisms, as Doc2 selectively affects only one particular form of STE: augmentation. Second, augmentation is partially due to Doc2-dependent superpriming of a subset of SVs (Fig. 8). Third, during augmentation, Doc2 is not an isolated $Ca^{2+}$ sensor, but rather forms a complex with at least one additional $Ca^{2+}$-binding protein, munc13.

**Different Forms of Short-Term Plasticity Are Mediated by Distinct Molecular Mechanisms.** The mechanisms that mediate short-term plasticity have been pursued for decades. As described above,

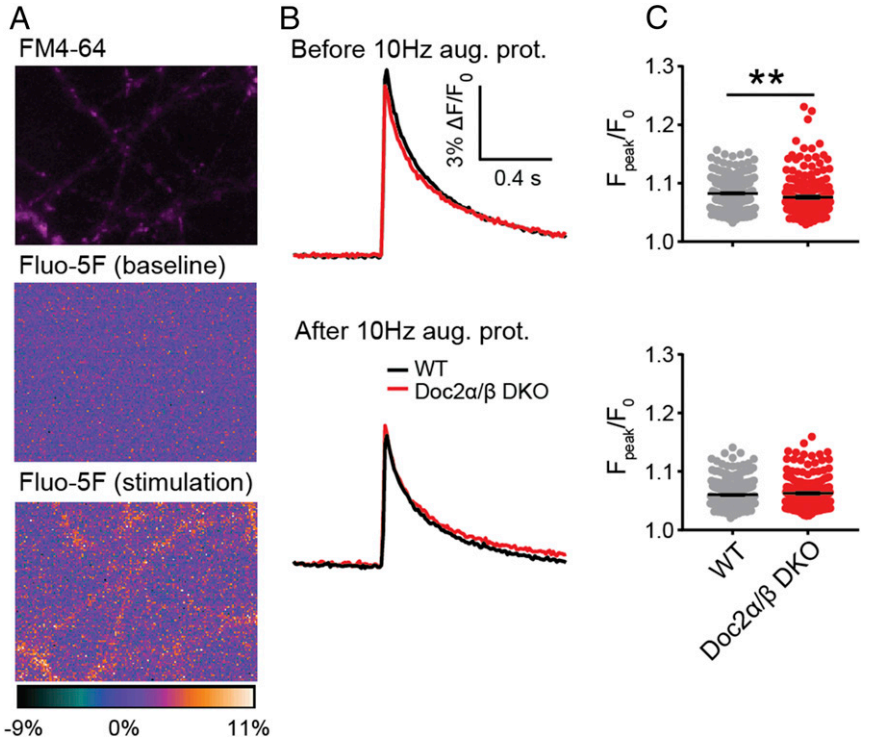


**Fig. 6.** Doc2-promoted augmentation is not mediated by changes in presynaptic $Ca^{2+}$ dynamics. (*A*) Image of a representative neuron loaded with FM4-64 (magenta), to identify synaptic boutons, and Fluo-5F (heat map), to measure changes in $[Ca^{2+}]_i$. (*B*) Averaged Fluo-5F $\Delta F/F_0$ versus time traces in response to a single stimulation 5 s before (*Upper*) and 5 s after (*Lower*) the augmentation protocol were imaged using WT (340 boutons, four independent litters of mice) or Doc2α/β DKO (214 boutons, four independent litters of mice) neurons. (*C*) Scatterplots of $F_{peak}/F_0$ quantified from individual boutons. $^{**}P < 0.01$, unpaired *t* test.

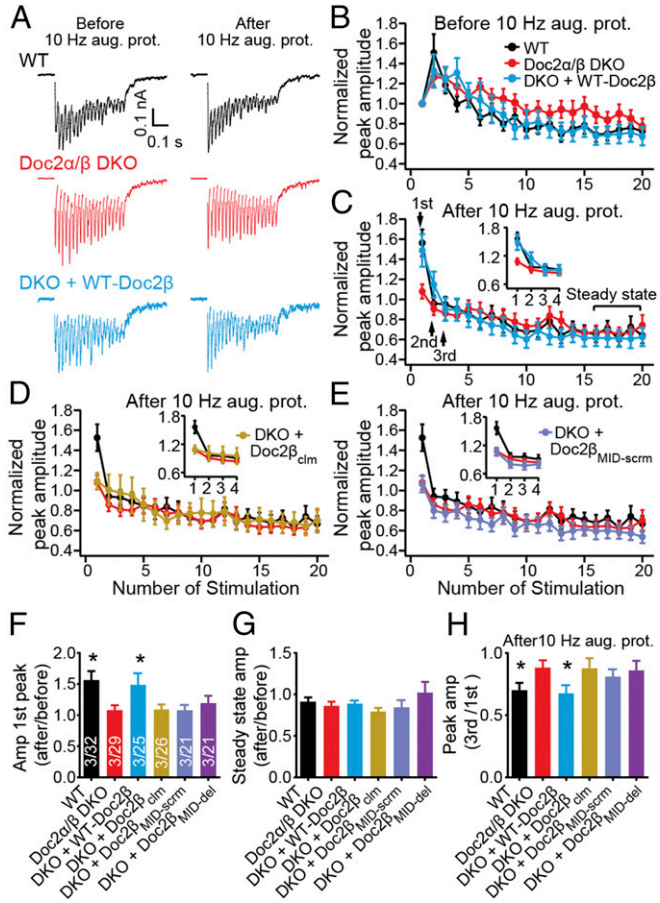


**Fig. 7.** Doc2 mediates synaptic augmentation by enhancing SV superpriming. (*A*) A 40-Hz stimulus train (0.5 s) was delivered 20 s before (*Left*) and 5 s after (*Right*) the augmentation protocol. (*B–E*) The peak amplitude of each EPSC during the two 40-Hz trains before (*B*) and after (*C–E*) applying the augmentation protocol was normalized to the first EPSC before augmentation. Data are plotted as mean ± SEM versus the stimulus number. In the first three EPSCs after the augmentation protocol (*Inset*), depression was steeper in WT versus Doc2α/β DKO neurons while steady-state amplitudes remained the same. These results indicate fewer superprimed SVs in the DKO. Expression of WT-Doc2β (*C*), but not $Doc2\beta_{clm}$ (*D*) or $Doc2\beta_{MID\text{-}scrm}$ (*E*), rescued the superpriming phenotype. (*F* and *G*) Normalized peak amplitude of each first response (*F*) and steady-state responses (*G*) before and after the augmentation protocol are presented as mean ± SEM. (*H*) After the augmentation protocol, the extent of SV superpriming was estimated by dividing the amplitude of the third peak by the first peak. Data are shown as mean ± SEM. $*P < 0.05$ versus Doc2α/β DKO, Kruskal–Wallis test followed by Dunn's post hoc test.

three different forms of STE (PPF, augmentation, and PTP) are classified based on their timescales; it is unclear whether they are mediated via the same or distinct molecular mechanisms. The experiments reported here shed light on this question.

Both augmentation and PTP are induced by trains of stimulation, but PTP requires higher stimulation frequencies and lasts longer than augmentation. Therefore, comparing these two forms of plasticity may reveal critical information regarding mechanisms underlying STP. In the present study, we show that in cultured hippocampal neurons, augmentation results from SV superpriming. Interestingly, it was reported that PTP also requires superpriming (34). However, Doc2 is involved in augmentation but not PTP, so the underlying molecular mechanisms must be at least partially distinct. Consistent with this idea, it has been reported that a mutant form of $Ca_v2.1$, which is the α-subunit of P/Q type $Ca^{2+}$ channels, affects augmentation but not PTP (47). Since both augmentation and PTP are driven by $Ca^{2+}$ that accumulates in presynaptic nerve terminals during bouts of activity, we speculate that there is a $[Ca^{2+}]_i$ threshold that separates these two forms of STE. Doc2-dependent augmentation occurs when the presynaptic $[Ca^{2+}]_i$ remains below this threshold. Once presynaptic $[Ca^{2+}]_i$ exceeds the threshold, a Doc2-independent mechanism is engaged and drives PTP. The molecular mechanisms underlying PTP, and how synapses switch between augmentation and PTP, remain obscure and require further study.

**Doc2 Superprimes a Subset of SVs in RRP During Augmentation.** There are conflicting reports as to whether the size of the RRP increases (12) or does not change (10) during augmentation. Using two independent methods (Fig. 5 and *SI Appendix*, Figs. S9 and S10), we found that the size of RRP stays constant when synapses are augmented. Hence, augmentation should rely mainly on an increase in $P_{vr}$. This could result from increases in $Ca^{2+}$ influx, but our $Ca^{2+}$ measurements argue against this possibility (Fig. 6). Rather, our findings strongly indicate that the increase in $P_{vr}$ during augmentation results from an increase in the number of superprimed SVs, and we identify Doc2 as a mediator of this process. Moreover, munc13, a Doc2-binding protein, has also been shown to be functionally involved in superpriming (48–50). We found that interactions with munc13 were crucial for Doc2 to drive augmentation. In response to $Ca^{2+}$ entry, Doc2 mediates munc13-1 translocation to the plasma membrane and might also alter the conformation or positioning of munc13 at release sites. We propose a model in which the Doc2–munc13 complex is recruited to the plasma membrane by $Ca^{2+}$ during train stimulation, consequently driving superpriming of a subset of SVs in the RRP, to enhance $P_{vr}$ (Fig. 8). Interestingly, the amount of time that Doc2 spends at the plasma membrane coincides with the duration of augmentation; stronger stimulation does not significantly affect this dwell time. These properties might tune Doc2 to specifically regulate synaptic augmentation, as opposed to other forms of STP.

**A Protein Complex Serves as the $Ca^{2+}$ Sensor for Augmentation.** As described above, we propose that Doc2 and munc13 form the core of an "augmentation complex" that senses presynaptic $Ca^{2+}$ signals to regulate this specific form of STP (Fig. 8). We note that both munc13-1 and munc13-2 (11, 12) bind Doc2 (19), so either isoform could potentially support augmentation. This complex is also likely to contain additional components, including the ubiquitous $Ca^{2+}$-binding protein calmodulin. Calmodulin forms direct contacts with munc13, and when this interaction was disrupted via mutations in munc13, reductions in synaptic augmentation were observed (12). We note that disruption of Doc2–munc13 interactions (Fig. 2*G*, *Lower*), or of calmodulin–munc13 interactions (12), did not completely abolish augmentation. Therefore, it is likely that either of these complexes (Doc2–munc13 or calmodulin–munc13) is sufficient to drive some degree of synaptic augmentation, independent of the other complex. This model predicts that to abolish augmentation it will be necessary to disrupt both complexes. Another possibility is that Doc2, munc13, and calmodulin form a three-component complex that functions as the $Ca^{2+}$ sensor for augmentation; all three components are needed for optimal function, but partial function is preserved when individual interactions are disrupted. Since Doc2 and calmodulin bind to different regions of munc13 (12, 19), we favor the latter, three-component, model.

Since Doc2 and munc13 have a number of additional binding partners (42, 51–53), it remains possible that the augmentation complex contains additional proteins. Regardless, the data reported here demonstrate that Doc2 is part of a $Ca^{2+}$-sensing complex for augmentation; it directly binds $Ca^{2+}$ via its C2B domain to help mediate augmentation.

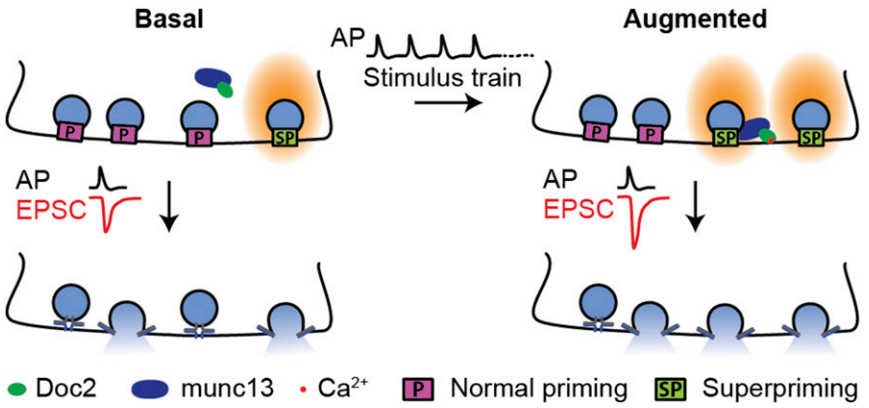


**Fig. 8.** Model of Doc2-dependent synaptic augmentation. In basal conditions, only a small portion of SVs in the RRP are superprimed. Augmentation is induced when synapses are stimulated by a series of action potentials (APs), resulting in the accumulation of residual $Ca^{2+}$. This $Ca^{2+}$ binds to the C2B domain of Doc2, triggering the translocation of the Doc2–munc13 complex to the plasma membrane. At the plasma membrane, the complex drives superpriming of a subset of SVs.

## Materials and Methods

**cDNA Constructs.** cDNA encoding the C2AB domain of mouse Doc2β (amino acids 125–412) was provided by M. Verhage, Vrije Universiteit, Amsterdam. To generate a full-length cDNA, the N-terminal segment (amino acids 1–124) of rat Doc2β was synthesized and appended onto the C2AB domain using splice overlap extension PCR as previously described (28). N-terminal domains encoding the scrambled and MID deletion mutants were also synthesized and fused to the C2AB domain, resulting in $Doc2\beta_{MID\text{-}scrm}$ and $Doc2\beta_{MID\text{-}del}$. $Doc2\beta_{clm}$ was generated using QuikChange Site-Directed Mutagenesis (Agilent Technologies) as previously described (30). To generate N-terminal GFP fusion proteins, each Doc2β construct was subcloned into pAcGFP1-C1. To generate lentiviral constructs, each Doc2β template was subcloned into pLOX [SynDsRed(W)-Syn-GFP(W)]. The EGFP-tagged munc13-1 plasmid was obtained from N. Brose, Max Plank Institute for Experimental Medicine, Gottingen, Germany, and the EGFP in this plasmid was replaced with mCherry to generate a munc13-1–mCherry fusion protein.

**Hippocampal Neuron Culture.** The Doc2α/β DKO mouse colony was generated by crossing Doc2α KO mice and Doc2β KO mice; both lines were provided by M. Verhage. Hippocampal neurons were cultured from mice at postnatal day 0 or from rats at embryonic day 18. Dissections were performed in accordance with the guidelines of the National Institutes of Health, as approved by the Animal Care and Use Committee of the University of Wisconsin–Madison. Briefly, rodent hippocampi were isolated in ice-cold Hank's buffered salt solution (Corning) and digested in 0.25% Trypsin (Corning) at 37 °C. After a 30-min incubation, the tissue was mechanically dissociated in DMEM with 10% FBS (Thermo Scientific). Cells were plated on poly-D-lysine precoated glass coverslips (Warner Instruments) at a density of 25,000–40,000 cells/$cm^2$. Cultures were maintained in Neurobasal-A culture medium with 2% B27 and 2 mM GlutaMAX (Life Technologies) at 37 °C in a 5% $CO_2$ humidified incubator.

**Live Cell Imaging.** Rat hippocampal neurons, PC12 cells, or HEK293T cells were cotransfected with Doc2β-GFP constructs and the munc13-1–mCherry construct, using calcium phosphate. Rat hippocampal neurons were transfected after 5 d of culture (5 DIV), while PC12 and HEK293T cells were transfected when they reached 70–80% confluency. Transfected cells were imaged 24–48 h after transfection. For live cell imaging, the coverslips were transferred to an imaging buffer (145 mM NaCl, 2.8 mM KCl, 1 mM $MgCl_2$, 1.2 mM $CaCl_2$, 10 mM glucose, and 10 mM Hepes–NaOH, pH 7.3). To trigger translocation, neurons or PC12 cells were perfused with depolarization buffer (87.8 mM NaCl, 60 mM KCl, 1 mM $MgCl_2$, 1.2 mM $CaCl_2$, 10 mM glucose, and 10 mM Hepes–NaOH, pH 7.3) using the Octaflow 2 perfusion system (ALA Scientific). In some experiments, neurons were transfected with only Doc2β-GFP and preincubated with $Ca^{2+}$ indicator X-Rhod-1 AM (1 μM, 15 min). These neurons were stimulated with voltage steps (~40 V, 1 ms), using a bipolar electrode pulled from theta glass capillary tubing (Warner Instruments) and filled with imaging buffer. Individual cells were imaged with an Olympus IX83 inverted microscope with an Olympus 60×/1.49 Apo N objective, a Hamamatsu Orca Flash4.0 CMOS camera, and an X-Cite 120LED light source controlled by MetaMorph software (Molecular Devices). Cells were imaged for 25 s; an image from each channel, in series, was acquired every 1 s (0.5 s/channel). Fluorescence intensity over time, for a region of interest, was quantified using the ImageJ Plugin Time Series Analyzer. Translocation was quantified by calculating the plasma membrane (PM) to cytosol (C) ratio of fluorescence intensity as described in *SI Appendix*, Fig. S3.

HEK293T cells were used for PMA-induced translocation experiments. Individual cells were identified and imaged using an Olympus FV1000 confocal microscope. Images were acquired before and 5 min after incubation in 0.1 μM PMA.

**$Ca^{2+}$ Imaging.** Cultured hippocampal neurons (13–15 DIV) from WT or Doc2α/β DKO KO mice were depolarized with 40 mM KCl and loaded with 14.8 μM FM4-64 (Thermo Scientific, 10 min incubation) to label synaptic boutons. Cells were then washed with artificial cerebrospinal fluid containing 1 mM ADVASEP-7 (Sigma) and loaded with 13.6 μM of Fluo-5F AM (with 1% Pluronic F-127; Thermo Scientific) for 10 min, washed, and transferred to a field stimulation chamber. Imaging was performed using the inverted microscope described above. Fields of view were chosen to maximize the number of boutons (visualized by FM4-64) on isolated processes, taking care to avoid glia (identifiable by morphology, kinetics of evoked $Ca^{2+}$ responses, and high resting $Ca^{2+}$ signal). Single-action potential $Ca^{2+}$ transients were measured before and after the augmentation-induction protocol (10 Hz, 5 s). Images were acquired at 100 Hz (10 ms exposure time), with 2 × 2 pixel binning and 10% LED power (482 nm excitation). $Ca^{2+}$ responses from individual boutons were quantified in Fiji (43) and converted to $\Delta F/F_0$ (change in fluorescence divided by baseline fluorescence), and the peak of each response was extracted.

**Viral Infection.** To generate lentivirus, HEK 293T cells were cotransfected with a pLOX construct and two viral packaging vectors (vesicular stomatitis virus G glycoprotein and Delta 8.9). After 2 d, lentivirus particles were harvested from the HEK cell culture media by centrifugation at 82,700 × *g* for 2 h. Hippocampal neurons were infected with lentivirus at 5 DIV and used for electrophysiological recordings at 13–17 DIV. Since expression was not apparent in all cells, infected neurons were visually identified by GFP fluorescence.

**Electrophysiology.** EPSCs were recorded from cultured mouse hippocampal neurons via whole-cell patch-clamp using a MultiClamp 700B amplifier (Molecular Devices). During recordings, neurons were maintained at room temperature and continuously perfused with a bath solution consisting of 128 mM NaCl, 5 mM KCl, 2 mM $CaCl_2$, 1 mM $MgCl_2$, 30 mM glucose, 50 μM D-AP5, 20 μM bicuculline, and 25 mM Hepes, pH 7.3. Postsynaptic neurons were voltage-clamped at −70 mV with a recording pipette with resistances of 3–5 MΩ. The recording pipettes were filled with a pipette solution consisting of 130 mM K-gluconate, 1 mM EGTA, 5 mM Na-phosphocreatine, 2 mM Mg-ATP, 0.3 mM Na-GTP, 5 mM QX-314, and 10 mM Hepes, pH 7.3. Only cells with series resistances of <15 MΩ were used for recordings. For evoked EPSCs, presynaptic neurons were stimulated with a voltage step from 0 to ~40 V for 1 ms, using the same electrode as in live cell imaging described above, but filled with bath solution. To measure the RRP, whole-cell patched neurons were locally perfused with bath solution plus 500 mM sucrose for 8 s using a Picospritzer III (Parker). For EGTA-AM experiments, neurons were preincubated in 100 μM EGTA-AM (EMD Millipore) for 20 min before recording. To test the effect of CTZ, EPSCs were recorded from the same cell

before and after perfusion with 100 μM CTZ (Sigma). Data were acquired using pClamp software (Molecular Devices), sampled at 10 kHz, and filtered at 2.8 kHz. Data analysis was performed using Clampfit (Molecular Devices) and Igor (WaveMetrics) software. D-AP5, bicuculline, and QX-314 were purchased from TOCRIS Bioscience (R&D Systems).

**Immunoblot Analysis.** At 13–15 DIV, cultured neurons were harvested using lysis buffer (1× PBS with 10 mM EGTA, 1% Triton X-100, 2% SDS, 0.5% PMSF, 0.5 mg/mL leupeptin, 0.7 mg/mL pepstatin, 1 mg/mL aprotinin, pH 7.4) and centrifuged at 13,400 × *g* for 10 min in 4 °C. Supernatants (10 μg) were subjected to SDS/PAGE and immunoblot analysis using a nonisoform-specific anti-Doc2 chicken polyclonal antibody (Covance; 1:50 dilution). To ensure equal loading, blots were also probed with a mouse polyclonal antibody against valosin-containing protein (Abcam; 1:800 dilution). Immunoreactive bands were visualized using HRP-conjugated anti-chicken (Abcam; 1:2,000 dilution) or anti-mouse (Abcam; 1:2,000 dilution) secondary antibodies and Super Signal West Pico Chemiluminescent Substrate (Thermo Fisher).

**Statistical Analysis.** In all of the electrophysiology experiments, the number of independent litters, *N*, and the number of cells or recordings, *n*, are indicated in the figures as *N*/*n*. Due to the poor normality of these data, nonparametric multiple comparisons using a Kruskal–Wallis test, followed by Dunn's post hoc test, was conducted to evaluate significance. For comparison of two groups, differences were assessed with unpaired two-tailed Student's *t* tests or the Mann–Whitney *U* test. Statistical analysis was performed using Prism 6 software (GraphPad).

**ACKNOWLEDGMENTS.** We thank E. Neher for suggesting experiments and all members of the E.R. Chapman laboratory for critical comments regarding this manuscript. This study was supported by National Institute of Health Grants MH061876 and NS097362 (to E.R.C.), and GM118801 (to R.A.P.). D.A.R. was supported by National Science Foundation Graduate Research Fellowship Program Grant DGE-1256259 and Neuroscience Training Program Grant T32-GM007507. E.R.C. is an Investigator of the Howard Hughes Medical Institute.

1. Zucker RS, Regehr WG (2002) Short-term synaptic plasticity. *Annu Rev Physiol* 64: 355–405.
2. Hansel D, Mato G (2013) Short-term plasticity explains irregular persistent activity in working memory tasks. *J Neurosci* 33:133–149.
3. Mongillo G, Barak O, Tsodyks M (2008) Synaptic theory of working memory. *Science* 319:1543–1546.
4. Nadim F, Manor Y (2000) The role of short-term synaptic dynamics in motor control. *Curr Opin Neurobiol* 10:683–690.
5. Pan B, Zucker RS (2009) A general model of synaptic transmission and short-term plasticity. *Neuron* 62:539–554.
6. Holohean AM, Magleby KL (2011) The number of components of enhancement contributing to short-term synaptic plasticity at the neuromuscular synapse during patterned nerve stimulation progressively decreases as basal release probability is increased from low to normal levels by changing extracellular Ca2+. *J Neurosci* 31: 7060–7072.
7. Thomson AM (2000) Facilitation, augmentation and potentiation at central synapses. *Trends Neurosci* 23:305–312.
8. Kamiya H, Zucker RS (1994) Residual Ca2+ and short-term synaptic plasticity. *Nature* 371:603–606.
9. Jackman SL, Turecek J, Belinsky JE, Regehr WG (2016) The calcium sensor synaptotagmin 7 is required for synaptic facilitation. *Nature* 529:88–91.
10. Stevens CF, Wesseling JF (1999) Augmentation is a potentiation of the exocytotic process. *Neuron* 22:139–146.
11. Rosenmund C, et al. (2002) Differential control of vesicle priming and short-term plasticity by Munc13 isoforms. *Neuron* 33:411–424.
12. Junge HJ, et al. (2004) Calmodulin and Munc13 form a Ca2+ sensor/effector complex that controls short-term synaptic plasticity. *Cell* 118:389–401.
13. Shin OH, et al. (2010) Munc13 C2B domain is an activity-dependent Ca2+ regulator of synaptic exocytosis. *Nat Struct Mol Biol* 17:280–288.
14. Klyachko VA, Stevens CF (2006) Temperature-dependent shift of balance among the components of short-term plasticity in hippocampal synapses. *J Neurosci* 26:6945–6957.
15. Klyachko VA, Stevens CF (2006) Excitatory and feed-forward inhibitory hippocampal synapses work synergistically as an adaptive filter of natural spike trains. *PLoS Biol* 4:e207.
16. Kandaswamy U, Deng PY, Stevens CF, Klyachko VA (2010) The role of presynaptic dynamics in processing of natural spike trains in hippocampal synapses. *J Neurosci* 30: 15904–15914.
17. Kalkstein JM, Magleby KL (2004) Augmentation increases vesicular release probability in the presence of masking depression at the frog neuromuscular junction. *J Neurosci* 24:11391–11403.
18. Augustin I, Rosenmund C, Südhof TC, Brose N (1999) Munc13-1 is essential for fusion competence of glutamatergic synaptic vesicles. *Nature* 400:457–461.
19. Orita S, et al. (1997) Physical and functional interactions of Doc2 and Munc13 in Ca2+-dependent exocytotic machinery. *J Biol Chem* 272:16081–16084.
20. Orita S, et al. (1995) Doc2: A novel brain protein having two repeated C2-like domains. *Biochem Biophys Res Commun* 206:439–448.
21. Kojima T, Fukuda M, Aruga J, Mikoshiba K (1996) Calcium-dependent phospholipid binding to the C2A domain of a ubiquitous form of double C2 protein (Doc2 beta). *J Biochem* 120:671–676.
22. Yao J, Gaffaney JD, Kwon SE, Chapman ER (2011) Doc2 is a Ca2+ sensor required for asynchronous neurotransmitter release. *Cell* 147:666–677.
23. Groffen AJ, et al. (2010) Doc2b is a high-affinity Ca2+ sensor for spontaneous neurotransmitter release. *Science* 327:1614–1618.
24. Pang ZPP, et al. (2011) Doc2 supports spontaneous synaptic transmission by a Ca(2+)-independent mechanism. *Neuron* 70:244–251.
25. Bacaj T, et al. (2013) Synaptotagmin-1 and synaptotagmin-7 trigger synchronous and asynchronous phases of neurotransmitter release. *Neuron* 80:947–959.
26. Sakaguchi G, et al. (1999) Doc2alpha is an activity-dependent modulator of excitatory synaptic transmission. *Eur J Neurosci* 11:4262–4268.
27. Groffen AJA, Friedrich R, Brian EC, Ashery U, Verhage M (2006) DOC2A and DOC2B are sensors for neuronal activity with unique calcium-dependent and kinetic properties. *J Neurochem* 97:818–833.
28. Gaffaney JD, Xue R, Chapman ER (2014) Mutations that disrupt $Ca^{2+}$-binding activity endow Doc2β with novel functional properties during synaptic transmission. *Mol Biol Cell* 25:481–494.
29. Groffen AJA, et al. (2004) Ca(2+)-induced recruitment of the secretory vesicle protein DOC2B to the target membrane. *J Biol Chem* 279:23740–23747.
30. Xue R, Gaffaney JD, Chapman ER (2015) Structural elements that underlie Doc2β function during asynchronous synaptic transmission. *Proc Natl Acad Sci USA* 112: E4316–E4325.
31. Friedrich R, Gottfried I, Ashery U (2013) Munc13-1 translocates to the plasma membrane in a Doc2B- and calcium-dependent manner. *Front Endocrinol (Lausanne)* 4:119.
32. Rhee JS, et al. (2002) Beta phorbol ester- and diacylglycerol-induced augmentation of transmitter release is mediated by Munc13s and not by PKCs. *Cell* 108:121–133.
33. Duncan RR, Betz A, Shipston MJ, Brose N, Chow RH (1999) Transient, phorbol ester-induced DOC2-Munc13 interactions in vivo. *J Biol Chem* 274:27347–27350.
34. Taschenberger H, Woehler A, Neher E (2016) Superpriming of synaptic vesicles as a common basis for intersynapse variability and modulation of synaptic strength. *Proc Natl Acad Sci USA* 113:E4548–E4557.
35. Trussell LO, Zhang S, Raman IM (1993) Desensitization of AMPA receptors upon multiquantal neurotransmitter release. *Neuron* 10:1185–1196.
36. Diamond JS, Jahr CE (1995) Asynchronous release of synaptic vesicles determines the time course of the AMPA receptor-mediated EPSC. *Neuron* 15:1097–1107.
37. Houy S, et al. (2017) Doc2B acts as a calcium sensor for vesicle priming requiring synaptotagmin-1, Munc13-2 and SNAREs. *eLife* 6:e27000.
38. Rosenmund C, Stevens CF (1996) Definition of the readily releasable pool of vesicles at hippocampal synapses. *Neuron* 16:1197–1207.
39. Schneggenburger R, Meyer AC, Neher E (1999) Released fraction and total size of a pool of immediately available transmitter quanta at a calyx synapse. *Neuron* 23:399–409.
40. Stevens CF, Williams JH (2007) Discharge of the readily releasable pool with action potentials at hippocampal synapses. *J Neurophysiol* 98:3221–3229.
41. Moulder KL, Mennerick S (2005) Reluctant vesicles contribute to the total readily releasable pool in glutamatergic hippocampal neurons. *J Neurosci* 25:3842–3850.
42. Calloway N, Gouzer G, Xue M, Ryan TA (2015) The active-zone protein Munc13 controls the use-dependence of presynaptic voltage-gated calcium channels. *eLife* 4:e07728.
43. Schindelin J, et al. (2012) Fiji: An open-source platform for biological-image analysis. *Nat Methods* 9:676–682.
44. Andrews-Zwilling YS, Kawabe H, Reim K, Varoqueaux F, Brose N (2006) Binding to Rab3A-interacting molecule RIM regulates the presynaptic recruitment of Munc13-1 and ubMunc13-2. *J Biol Chem* 281:19720–19731.
45. Kalla S, et al. (2006) Molecular dynamics of a presynaptic active zone protein studied in Munc13-1-enhanced yellow fluorescent protein knock-in mutant mice. *J Neurosci* 26:13054–13066.
46. Schlüter OM, Basu J, Südhof TC, Rosenmund C (2006) Rab3 superprimes synaptic vesicles for release: Implications for short-term synaptic plasticity. *J Neurosci* 26:1239–1246.
47. Mochida S, Few AP, Scheuer T, Catterall WA (2008) Regulation of presynaptic Ca(V)2.1 channels by Ca2+ sensor proteins mediates short-term synaptic plasticity. *Neuron* 57:210–216.
48. Lee JS, Ho WK, Neher E, Lee SH (2013) Superpriming of synaptic vesicles after their recruitment to the readily releasable pool. *Proc Natl Acad Sci USA* 110:15079–15084.
49. Ishiyama S, Schmidt H, Cooper BH, Brose N, Eilers J (2014) Munc13-3 superprimes synaptic vesicles at granule cell-to-basket cell synapses in the mouse cerebellum. *J Neurosci* 34:14687–14696.
50. Michelassi F, Liu H, Hu Z, Dittman JS (2017) A C1-C2 module in Munc13 inhibits calcium-dependent neurotransmitter release. *Neuron* 95:577–590.e5.
51. Verhage M, et al. (1997) DOC2 proteins in rat brain: Complementary distribution and proposed function as vesicular adapter proteins in early stages of secretion. *Neuron* 18:453–461.
52. Nagano F, et al. (1998) Interaction of Doc2 with tctex-1, a light chain of cytoplasmic dynein. Implication in dynein-dependent vesicle transport. *J Biol Chem* 273: 30065–30068.
53. Kaeser PS, et al. (2008) RIM1alpha and RIM1beta are synthesized from distinct promoters of the RIM1 gene to mediate differential but overlapping synaptic functions. *J Neurosci* 28:13435–13447.